

# Boundary-layer Suction and Aerodynamic Shape Optimization for Hybrid Laminar Flow Control on a Fin

Haoyang Wu<sup>1,2</sup>, Wenping Song<sup>1,2</sup>, Han Nie<sup>1,2</sup>, Zhonghua Han<sup>1,2</sup>

<sup>1</sup> Institute of Aerodynamic and Multidisciplinary Design Optimization, School of Aeronautics, Northwestern
Polytechnical University, Xi'an 710072, China

<sup>2</sup> National Key Laboratory of Aircraft Configuration Design, Xi'an 710072, China

#### **Abstract**

Aerodynamic drag reduction is essential for improving flight efficiency and reducing emissions of transport aircraft, and is of great significance for achieving the goal of green aviation. Application of hybrid laminar flow control (HLFC) system on fins has been proved of great potentials in drag reduction. How to design a good aerodynamic shape and boundary-layer suction distribution to reduce the sum of pressure drag and viscous friction drag by extending the laminar flow region under complex geometric constraints is still a challenge for HLFC on a highly swept fin. To address the problem, this article develops a surrogate-based HLFC fin design optimization method. The surrogate-based optimization is conducted based on an in-house software SurroOpt, and the aerodynamic characteristics of fins are calculated with a RANS solver PMNS3D coupled with automatic transition prediction by a  $N_{\text{TS}}$ - $N_{\text{CF}}$  e $^N$  method. Validation of the developed method is conducted on a 40°-swept fin at Ma=0.785 and Re=2.6×10 $^7$ , setting three suction areas over the fin surface at 0c~0.2c. The objective of the design optimization is to enlarge laminar flow region and reduce drag at a reasonable boundary-layer suction flow rate. Compared to the baseline fin with suction, whose laminar flow area is 41.25% and total drag is 35.46 counts at cruise state, the optimized fin has reached a larger laminar flow area of 57.7% and lower drag of 31.74 counts, and is more robust at  $\pm 2^\circ$  sideslip angles, suggesting that our method is effective for HLFC design on highly-swept fins.

**Keywords:** Hybrid laminar flow control, fin, surrogate-based optimization, Kriging model, e<sup>N</sup> method

### 1. Introduction

Reducing the drag of transport aircraft is beneficial for reducing carbon dioxide emissions and fuel consumption, and is important for achieving the goal of green aviation. For a high subsonic civil aircraft at cruise state, the friction drag accounts for 55% of the total drag. Due to the fact that the skin friction coefficient of laminar boundary layers is much lower than that of turbulent boundary layers, laminar flow design on aerodynamic components of an aircraft such as wings and fins can bring a significant decrease in the friction drag and improve the flight efficiency. Generally, there are three techniques to achieve laminar flow design: natural laminar flow (NLF), laminar flow control (LFC) and hybrid laminar flow control (HLFC) [1]. Among these techniques, the HLFC technique is capable of maintaining a large laminar flow region on a highly-swept wing or fin configuration with reasonable energy consumption and leads to significant drag reduction. Therefore, researches on the application of HLFC to wings and fins is of great significance to reducing energy consumption and emissions for future civil aircraft.

In the past few decades, a lot of wind tunnel and flight experiments have been conducted to prove the feasibility of applying HLFC to the vertical fin. Around 2000, Airbus installed the HLFC system on A320 fins and conducted flight tests<sup>[2]</sup>. The results show that the application of HLFC technique could maintain a large laminar flow region on the A320 fin<sup>[3]</sup>. Two years later, Europe carried out the ELFIN (European Laminar Flow Investigations) project<sup>[4]</sup> and focused on the research of flow mechanism and numerical method of HLFC. Wind tunnel experiments were also conducted as a validation. The experiment model was a backward-swept wing at a leading-edge swept angle of 28°. The results show that a laminar flow area of 43% could be achieved on the wing surface at a freestream Mach number of 0.7, by applying boundary-layer suction at 0%c~10%c of the wing near the leading edge. In 2013, Europe initiated the AFLoNEXT (Active Flow- Loads &Noise Control on Next Generation Wing) project, which further investigated a simplified suction system for HLFC<sup>[5]</sup> and installed the simplified suction system on A320 fins for numerical and experiment studies. The critical

N-factor for flow transition prediction was calibrated based on wind tunnel test results<sup>[6]</sup>, and flight tests were also conducted<sup>[7][8]</sup>. The results show that the predicted transition location on A320 fins were in good agreement with the experimental results, and a laminar area of 40% was observed at the cruise state as well as at ±2° sideslip angles<sup>[9]</sup>. In 2017, Yang et al<sup>[10]</sup> established a method to optimize the boundary layer suction distribution and aerodynamic shape for HLFC and carried out design optimizations on a wing. In summary, the current research mainly focuses on the design of HLFC suction system and aerodynamic shape optimization for HLFC design on wings, and there are few researches about design optimization for HLFC on highly-swept fins, where the crossflow instabilities are strong amplified near the leading edge.

The objective of this article is to develop a surrogate-based design optimization method for boundary-layer suction and aerodynamic shape optimization of a HLFC fin, in order to enlarge the laminar area and reduce drag with a reasonable suction flow rate. Besides, geometric constraints including the thicknesses at front and rear beams, and the maximum thickness of profile airfoils are taken into account, and the designed fin is expected to have robust aerodynamic performances at a certain sideslip angle.

This article continues in Chapter 2 on the description of flow solver coupled with an e<sup>N</sup> transition prediction method, as well as the framework of surrogate-based optimization. In Chapter 3, Design optimizations are conducted on a 40°-swept fin at Mach 0.785 and Re=2.6×10<sup>7</sup> to validate the developed method. Chapter 4 summarizes the work of this article and presents the outlook.

### 2. Methodology

# 2.1 Three-dimensional RANS equation solver coupled with e<sup>N</sup> transition prediction method

To evaluate the aerodynamic characteristics of a HLFC fin, an in-house three-dimensional compressible RANS equations solver PMNS3D<sup>[11]</sup>[12] [13]13] ,which with a  $N_{TS}/N_{CF}$  e<sup>N</sup> transition prediction module is adopted. The solver uses the finite volume method for spatial discretization and the LU-SGS method with multigrid acceleration. The turbulence model is SA model, and the flow transition onset is predicted by an e<sup>N</sup> method based on linear stability theory (LST). Wall normal velocity boundary condition is added to simulate the effect of boundary-layer flow suction. Under the parallel flow assumption, the LST-e<sup>N</sup> method assumes a small perturbation inside the boundary-layer, and solves the compressible linear stability equations to compute the spatial or temporal evolution of the perturbation. The perturbation is of the form:

$$q'(x,y,z,t) = \hat{q}(y) \cdot e^{(-\alpha_i x - \beta_i z)} e^{i(\alpha_r x + \beta_r z - \omega t)}, \tag{1}$$

where x, y, z are the coordinates of the streamline coordinate system; q' is the instantaneous perturbation of flow field variable;  $\hat{q}$  is the amplitude function of the perturbation;  $\omega$  is the circular frequency;  $\alpha_r$  and  $\beta_r$  are the wavenumbers of perturbations in the x- and z-directions;  $-\alpha_i$  and  $-\beta_i$  are the growth rates of perturbations in the x- and z-directions. The wave angle  $\varphi_w$  of perturbations is defined as the angle between the wave number vector and the direction of potential flow at the boundary layer edge. In addition, the Mack correlation of  $\beta_i = 0$  is added to solve the eigenvalue problem of linear stability equations<sup>[14]</sup>.

For Tollmien-Schlichting (TS) instabilities, the fixed wave angle method is used to calculate the amplification factors (also called *N* factors) of perturbations. The longitudinal TS waves at the wave angle of  $\varphi_w$ =0°, i.e., along the direction of potential flow velocity, are considered, and the *N* factors of TS waves are computed as follows.

$$N_{TS} = \int_{x_0}^{x} (-\alpha_i)_{f, \ \varphi_w = 0^{\circ}} dx$$
 (2)

For crossflow (CF) instabilities, the fixed spanwise wavenumber and fixed frequency method is used to calculate the N factors of perturbations. The stationary crossflow instabilities at the frequency of f = 0Hz are considered, and the N factors of CF waves are computed as follows.

$$N_{CF} = \int_{x_0}^{x} (-\alpha_i)_{f=0, \beta_r} dx$$
 (3)

### 2.2 The Surrogate-based optimization software: SurroOpt[16]

The core idea of surrogate-based optimization (SBO) is using historical data and surrogate model to guide the infilling of new samples. The main algorithms of SBO are Design of Experiment (DoE)<sup>[18]</sup>, surrogate modelling, infill sampling criterion and sub-optimization. Among these algorithms, infill sampling criterion and sub-optimization are the core mechanism of SBO, which ensure the sample points to be gathered around the global optimum and the optimization result is independent of initial samples and the global accuracy of surrogate model. Existing researches indicate that when solving expensive black-box problems in continuous and smooth design space, the efficiency of SBO is one or two order of magnitude higher than that of the methods directly using evolutionary algorithms such as genetic algorithm. In short, Surrogate-based optimization method is a kind of algorithm that make use of surrogate models to find the global optimum, solving the sub-optimization problem defined by infill-sampling criteria to produce new samples and repetitively updating the surrogate model until sample-point sequence converges to the global optimum. The flowchart of SurroOpt is shown in Figure 1, for more details, readers are recommended to refer to reference [16].

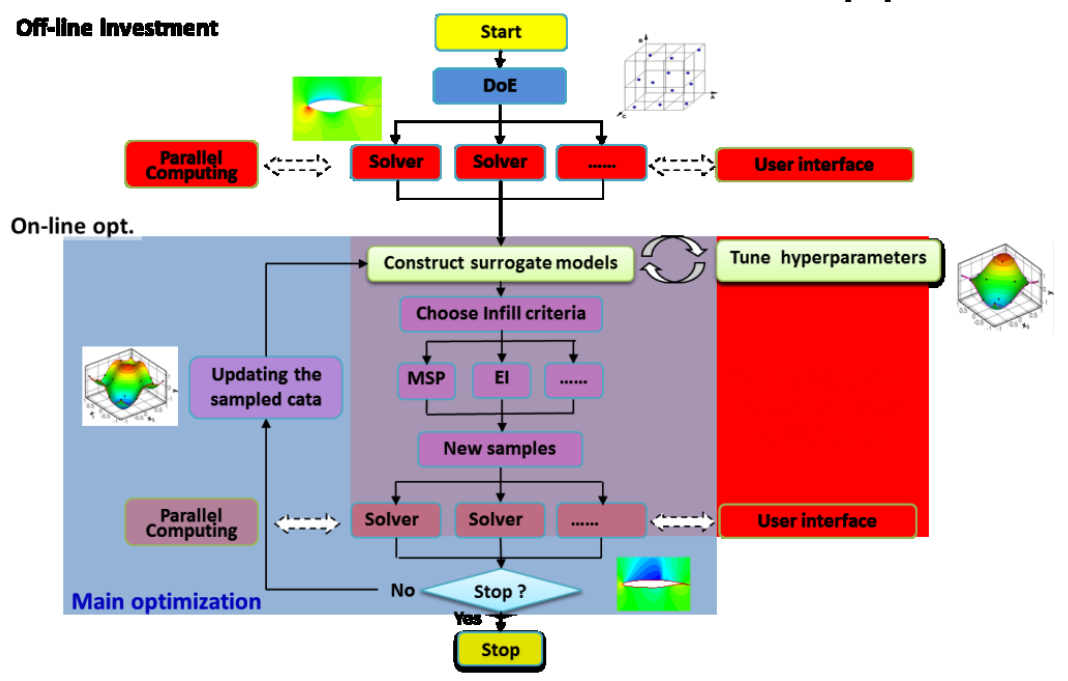


Figure 1 Flow chart of SurroOpt<sup>[16]</sup>

For design optimization of the HLFC fin of this paper, as shown in Figure 1, Latin hypercube sampling (LHS)<sup>[19]</sup> is used in the design of experiment (DOE), Kriging model and parallel sample infill criteria<sup>[20]</sup> of expected improvement (EI) criterion, minimum surrogate model prediction (MSP) criterion, lower confidence bound (LCB) criterion, probability of improvement(PI) criterion, and mean square error (MSE) criterion are used in sub-optimization. Hooke-Jeeves algorithm, Quasi-Newton Methods, and genetic algorithms are used to solve the sub-optimization problem. The procedures of a surrogate-based design optimization for HLFC fin are described as follows.

**Step 1** Set optimization objectives and constraints to establish an optimization model; Construct design variables by geometric parameterization method for the shape optimization, and by the suction coefficient for the suction control optimization;

**Step 2** DOE is conducted based on LHS method and initial samples are located within the design space. Responses of the initial samples are evaluated with PMNS3D, the responses at the initial sample points are used to establish the initial kriging models for objective functions and constraints, respectively:

**Step 3** The sub-optimizations are carried out by using EI, MSP, LCB, PI and MSE infill criteria. This process is called a sub optimization process and is the core mechanism of SBO methods. For

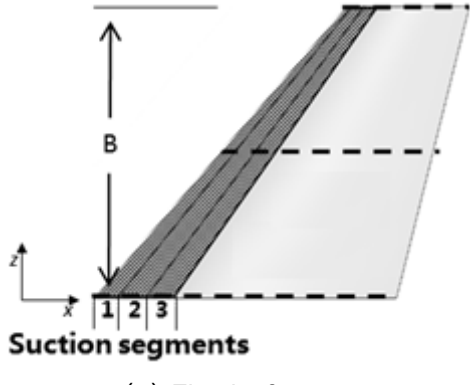
constrained optimization problems, in the optimization process, a surrogate model of the objective function is established and surrogate models for constraints are established at the same time;

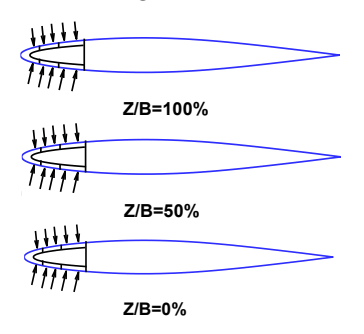
**Step 4** Obtain the response values of the sample points generated by each sub optimization using PMNS3D, add them to the sample point set, and rebuild the surrogate models. Repeat the above process until the convergence criteria are met and the optimization is terminated. The optimization convergence criteria used in this paper are the maximum number of CFD evaluations, the approximation accuracy of surrogate model at the optimum, the minimum value for maximum EI. If one of the convergence criteria is met, the optimization is terminated.

### 3. Design optimization of suction and aerodynamic shape parameters for HLFC on a fin

## 3.1 Evaluation of aerodynamic characteristics of the Baseline fin configuration

The surrogate-based design optimization method is applied to the boundary-layer suction and aerodynamic shape design of a HLFC fin. The baseline fin configuration has a root chord length of 5.2m, a span length of 5.03 m, a leading-edge swept angle of 40°, and a trailing edge swept angle of 14°. The planform of the fin and its airfoils at 3 typical sections spanwise are depicted in **Figure 2**. The boundary-layer flow suction is split into 3 segments chordwisely, locating within 0%c~6%c, 6%c~12%c and 12%c~20%c, respectively, and different suction coefficients are set for each segment. The suction coefficient is defined as:  $C_q = -(\rho_S V_S)/(\rho_\infty V_\infty)$ , in which the  $\rho_S$  represents the density at suction location and  $\rho_\infty$  represents the density of freestream;  $V_S$  represents the velocity normal to the airfoil surface at suction location, and  $V_\infty$  represents freestream velocity. The cruise state is Ma=0.785, H=10000m and Re=2.6×10<sup>7</sup> at a sideslip angle of  $\beta$ =0°.





(a) Fin planform

(b) Airfoils at root, mid-span and fin tip

Figure 2 Planform and section airfoils of the baseline fin with suction

In order to determine an appropriate computational grid for flow CFD evaluation, a grid convergence study is carried out. Five sets of computational grids are generated as: L0 (417 × 193 × 117), L1 (329 × 153 × 93), L2 (257 × 121 × 73), L3 (209 × 97 × 61), and L4 (169 × 81 × 49). The height of the first layer is set as  $6\times10^{-6}$  m to keep Y<sup>+</sup><1. **Figure 3** is a diagram of the computational grid, and **Figure 4** demonstrates the aerodynamic coefficients computed from the five sets of grids. The difference of drag coefficients between L0 and L1 is less than 1 count, and therefore the L1 grid is adopted in the following studies for aerodynamic characteristic evaluation.

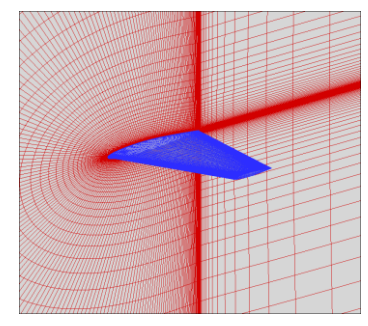


Figure 3 Diagram of the computational grid

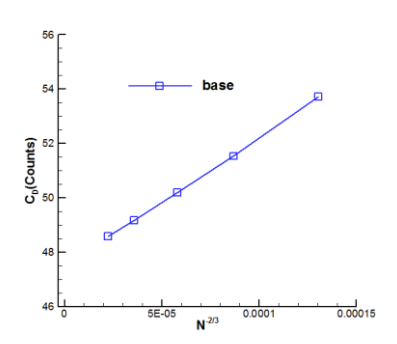


Figure 4 Calculated drag coefficients at different grid sizes

First, the aerodynamics of the baseline fin is evaluated without suction. The flow field of the baseline fin configuration is solved at the cruise state ( $\beta$ =0°) and at side-slip angles of  $\beta$ =1° and 2°. The pressure distributions over the fin surface are presented in **Figure 5**. A large range of moderate favorable pressure gradient is observed at the cruise state. Stability analysis is conducted on the baseline fin without suction and **Figure 6** shows that the *N* factors of crossflow instabilities are significantly amplified near the leading edge and result in flow transition. The transition prediction criterion is  $[N_{\text{tr_Ts}}, N_{\text{tr_CF}}]$ =[6.5, 7.5], referring to a former study by Schrauf et al<sup>[8]</sup>. **Figure 7** presents the predicted transition line over the fin surface. Due to the strong amplification of crossflow instabilities generated from the large leading-edge swept angle, the transition line is very close to the leading edge of fin without suction.

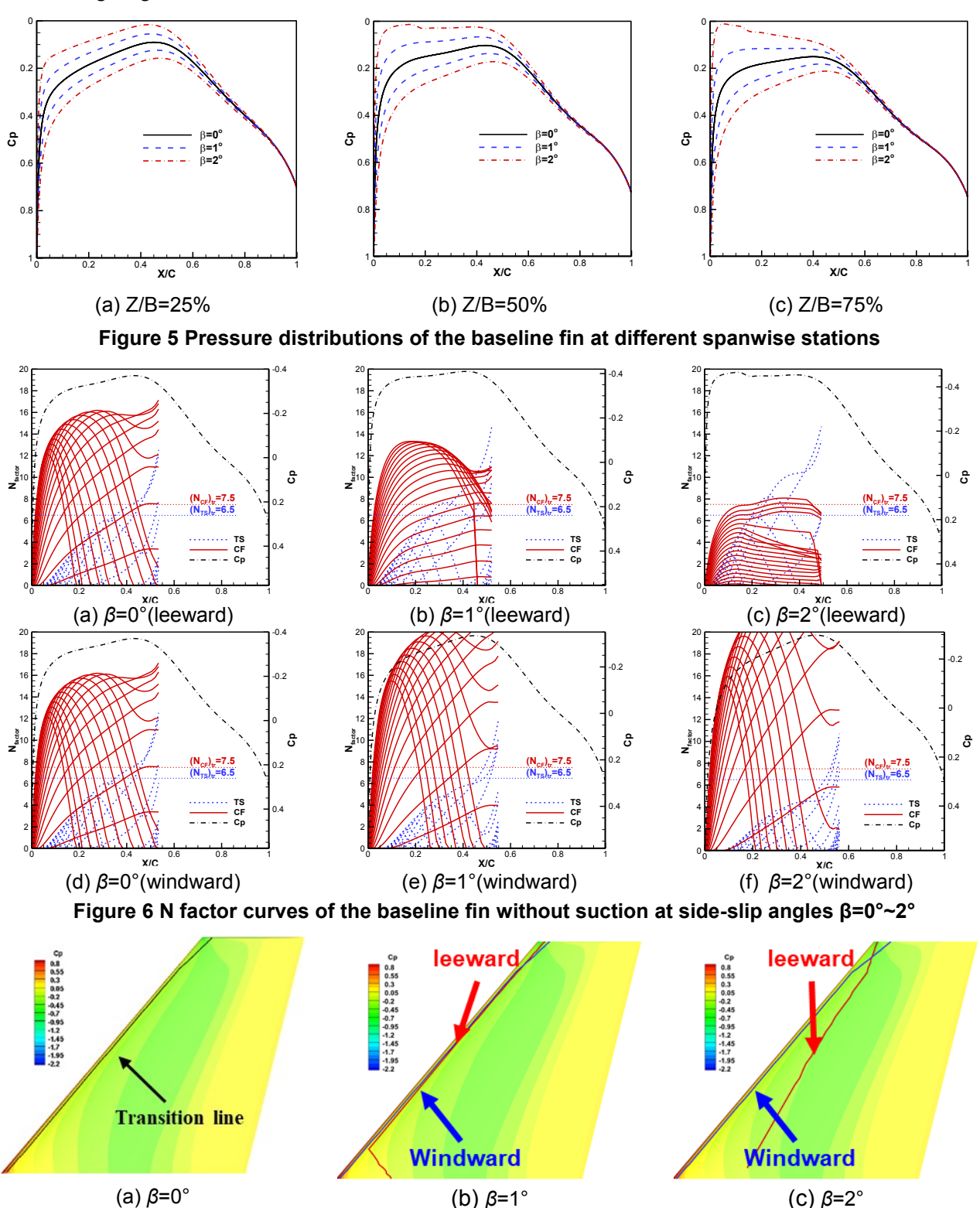


Figure 7 Transition lines of the baseline fin without suction at side-slip angles  $\beta$ =0°~2°

Then, the aerodynamics of the baseline fin is evaluated with suction. The flow field of the baseline fin configuration is solved and stability analyses are carried out. The suction coefficients in the three suction regions are  $C_{q1}$ =-0.0005583 at 0%c~6%c,  $C_{q2}$ =-0.0002053 at 6%c~12%c and  $C_{q3}$ =-0.0001444 at 12%c~20%c. The computed suction volume flow rate is  $Q_{V0}$ = 0.548m<sup>3</sup>/s and mass flow rate is  $Q_{M0}$ = 0.227kg/s. Figure 8 shows the *N* factor curves of TS and CF instabilities over the baseline fin surface with suction. It can be seen that due to the suction effect near the leading edge, the CF instabilities are significantly attenuated, and crossflow induced flow transition are avoided. Instead, flow transition is dominated by TS instabilities. Table 1 presents the aerodynamic characteristics of the baseline fin without and with suction. It can be seen that laminar flow area on the baseline fin can reach 41% at cruise state, bringing great benefits of reducing the friction drag. Whereas, the laminar flow potential hasn't been fully explored since that suction near the leading edge cannot attenuate the TS instabilities at the downstream regions. What's more, a stronger favorable pressure gradient is observed at the side-slip angle of  $\beta$ =2°, resulting in intense amplification of CF instabilities and early flow transition. Therefore, design optimization is required toward the suction distribution and aerodynamic shape of the baseline fin, in order to improve the aerodynamic characteristics at the cruise state as well as at certain side-slip angles.

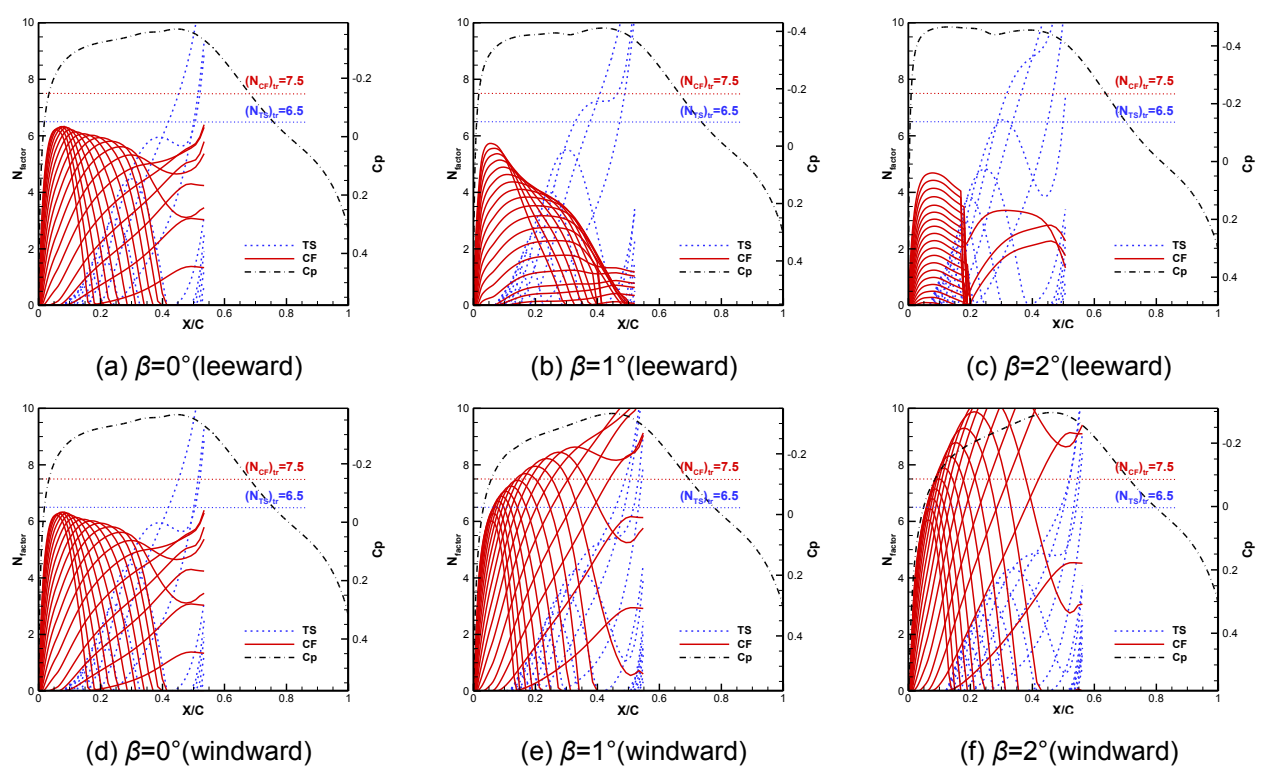


Figure 8 N factor curves of the baseline fin with suction at side-slip angles β=0°~2°

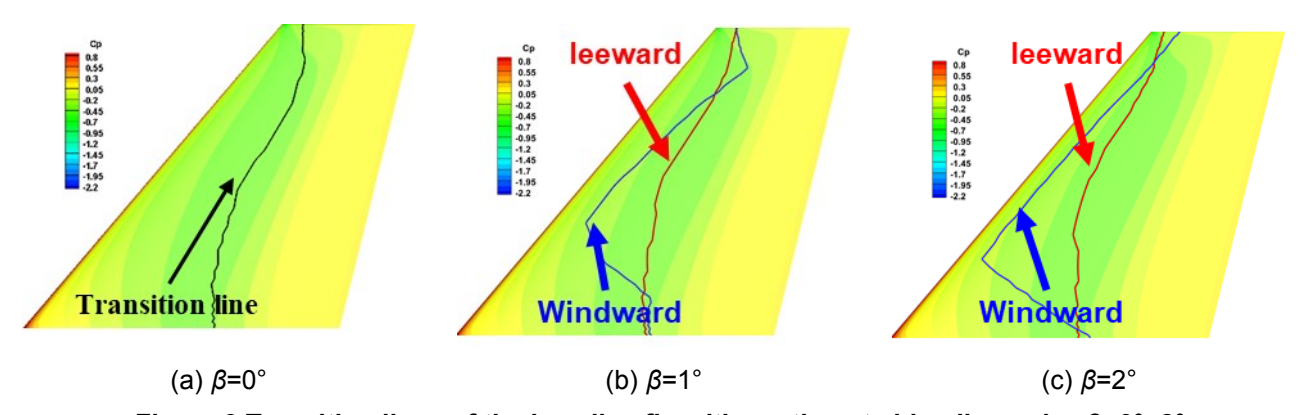


Figure 9 Transition lines of the baseline fin with suction at side-slip angles  $\beta=0^{\circ}-2^{\circ}$ 

| Table 1 Comparison of a | erodynamic characteristics of baseline | fin with and without suction |
|-------------------------|--|------------------------------|
|-------------------------|--|------------------------------|

| Configuration            | β (°) | Laminar area<br>(Upper Surface) | Laminar area (Lower Surface) | Drag coefficient (cts) |
|--------------------------|-------|---------------------------------|------------------------------|------------------------|
| Baseline without suction | 0     | 2.53%                           | 2.53%                        | 50.15                  |
|                          | 1     | 5.98%                           | 2.36%                        | 57.65                  |
|                          | 2     | 20.61%                          | 2.67%                        | 71.98                  |
| Baseline with suction    | 0     | 41.25%                          | 41.25%                       | 35.46                  |
|                          | 1     | 40.26%                          | 31.15%                       | 45.86                  |
|                          | 2     | 36.39%                          | 20.32%                       | 66.25                  |

### 3.2 Design optimization of suction and aerodynamic shape parameters of the HLFC fin

To address the problem that the TS instabilities are not well attenuated at the cruise state and the strong amplification of CF instabilities leads to early flow transition at certain side-slip angles, design optimization are carried out toward the suction and aerodynamic shape parameters of the fin. The taper ratio, aspect ratio and swept angle are kept unchanged. The profile airfoils at the fin root, middle and tip are designed, parameterized by an  $8^{th}$ -order CST<sup>[17]</sup> method, resulting in 27 geometric design variables. In addition, the suction coefficients at the three suction regions are also need to be determined, which comes to 3 design variables. The total number of design variables is 30. The design states are Ma=0.785,  $Re=2.6\times10^7$  and  $\beta=0^\circ$ ,  $2^\circ$ . The design objective is to enlarge the laminar flow region and reducing drag, at a reasonable suction flow rate. Geometric constraints are introduced to the maximum thickness of the airfoils as well as thicknesses at the front beam(25%c) and back beam(75%c) at the three spanwise stations, adding up to 9 geometric constraints. The optimization problem is described as follows.

$$\begin{aligned} & \min. \ 0.2 \times \left(\frac{Q}{Q_0}\right) + 0.4 \times \left(\frac{C_D}{C_{D0}}\right) + 0.4 / \left(\frac{S_L}{S_0}\right) \\ & s.t. \quad x_{tr,root} / c \leq 0.6 \\ & \quad x_{tr,z=0.5b} / c \leq 0.6 \\ & \quad S_{\beta=0^{\circ}} / S_{ref} \geq 0.45 \\ & \quad S_{\beta=2^{\circ}} / S_{ref} \geq 0.45 \\ & \quad t_{le,i} \geq t_{0,le,i} \\ & \quad t_{te,i} \geq t_{0,te,i} \\ & \quad t_{\max,i} \geq t_{0,\max,i} \\ & \quad i = 1, 2, 3 \end{aligned} \tag{4}$$

where  $Q_{\rm M}/Q_{\rm M0}$  represents the ratio of the suction mass flow rate of the designed and baseline fin,  $C_{\rm D}/C_{\rm D0}$  is the ratio of drag coefficients of the designed and baseline fin, and  $S_{\rm L}/S_{\rm 0}$  is the ratio of laminar flow area of the designed and baseline fin.  $x_{\rm tr,root}$  and  $x_{\rm tr,z=0.5b}$  represent the transition location at the fin root and middle section;  $S_{\beta=0^{\circ}}$  and  $S_{\beta=2^{\circ}}$  represent the laminar flow area of the designed wing at the side-slip angle of  $\beta=0^{\circ}$  and  $\beta=2^{\circ}$ ;  $t_{\rm le,i}$ ,  $t_{\rm te,i}$  and  $t_{\rm max,i}$  are thicknesses at the front beam and back beam, and the maximum thickness of airfoils at the three spanwise stations. Taking the Z/B=50% spanwise station as an example, the design space of profile airfoil and suction coefficients are presented in Figure 10, where "lower" and "upper" represent the boundary of design space. Within the design space, 52 initial samples are generated using the Latin hypercube sampling (LHS) method. The response values of these samples are calculated by PMNS3D, and Kriging models are established to conduct sub-optimization and search for the optimum. Two rounds of optimization were carried out, in the first round of the optimization design, a large number of design variables of the optimum was found to have reached the boundary of the design space, thus the design space

was expanded based on the optimum configuration of the first round, meanwhile the optimal configuration of the first round is taken as one of the initial samples of the second round; in addition, a part of samples of the first round are also taken as initial samples of the second round to speed up the process of the optimization and save the computational cost. Figure 11 depicted the convergence history of the optimization problem.

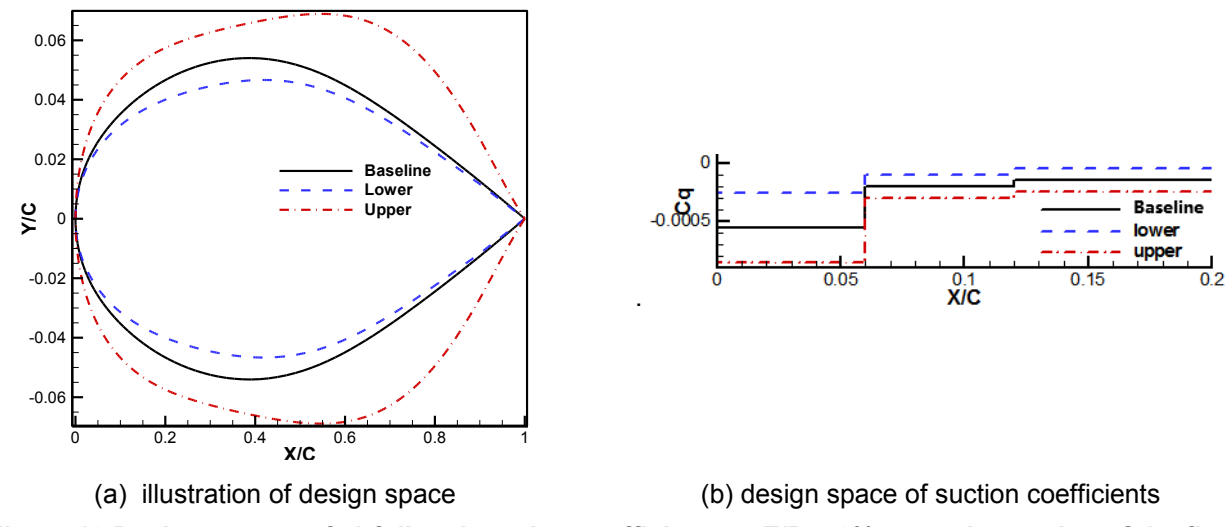


Figure 10 Design spaces of airfoil and suction coefficients at Z/B=50% spanwise station of the fin

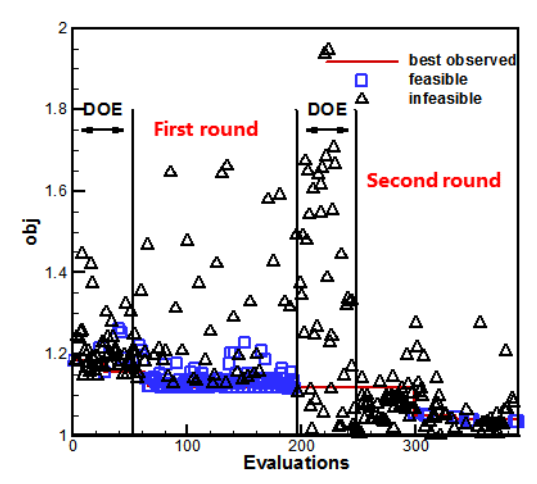
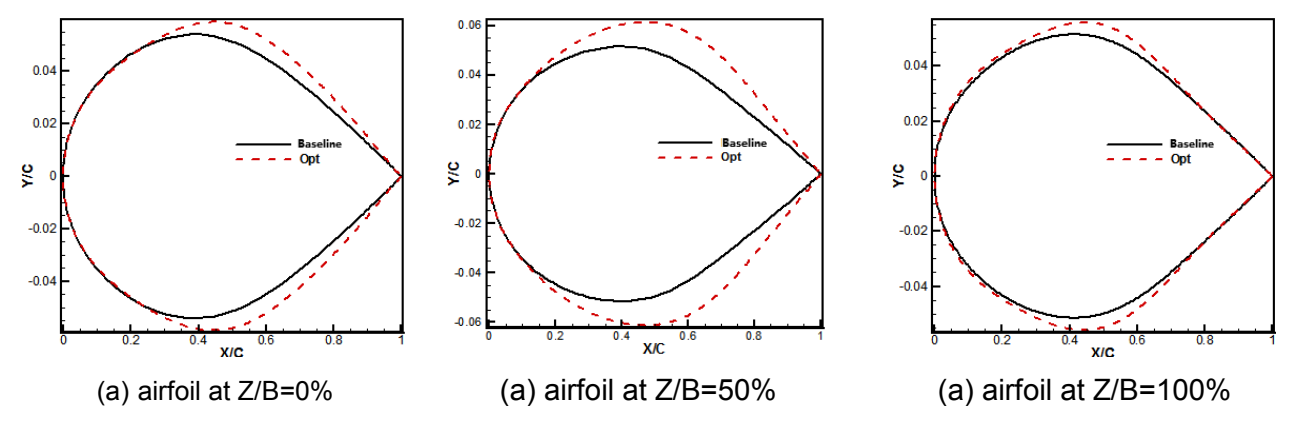


Figure 11 Convergence history of the two-round design optimization of HLFC fin

The profile airfoils and suction coefficients of the optimized fin is shown in **Figure 12**. Compared with the baseline fin, the maximum thickness location moves toward the trailing edge. The reason is the increase of favorable pressure gradient region in order to better attenuate TS instabilities. The suction coefficients in the three suction regions of the optimized fin are  $C_{q1}$ =-0.0007418 at 0%c~6%c,  $C_{q2}$ =-0.0002634 at 6%c~12%c and  $C_{q3}$ =-0.0002034 at 12%c~20%c. The corresponding suction volume flow rate is  $Q_V$ = 0.731m³/s and mass flow rate is  $Q_M$ = 0.302kg/s, which are larger than those on the baseline fin and are expected to better attenuate the crossflow instabilities.



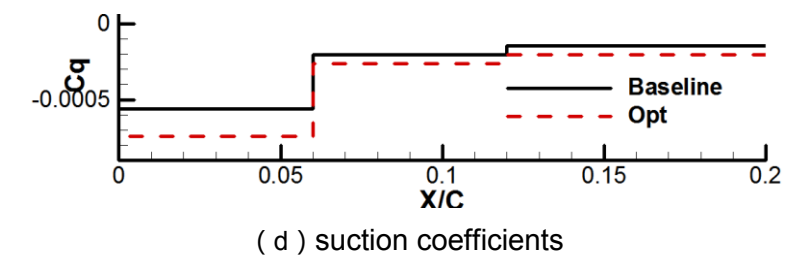
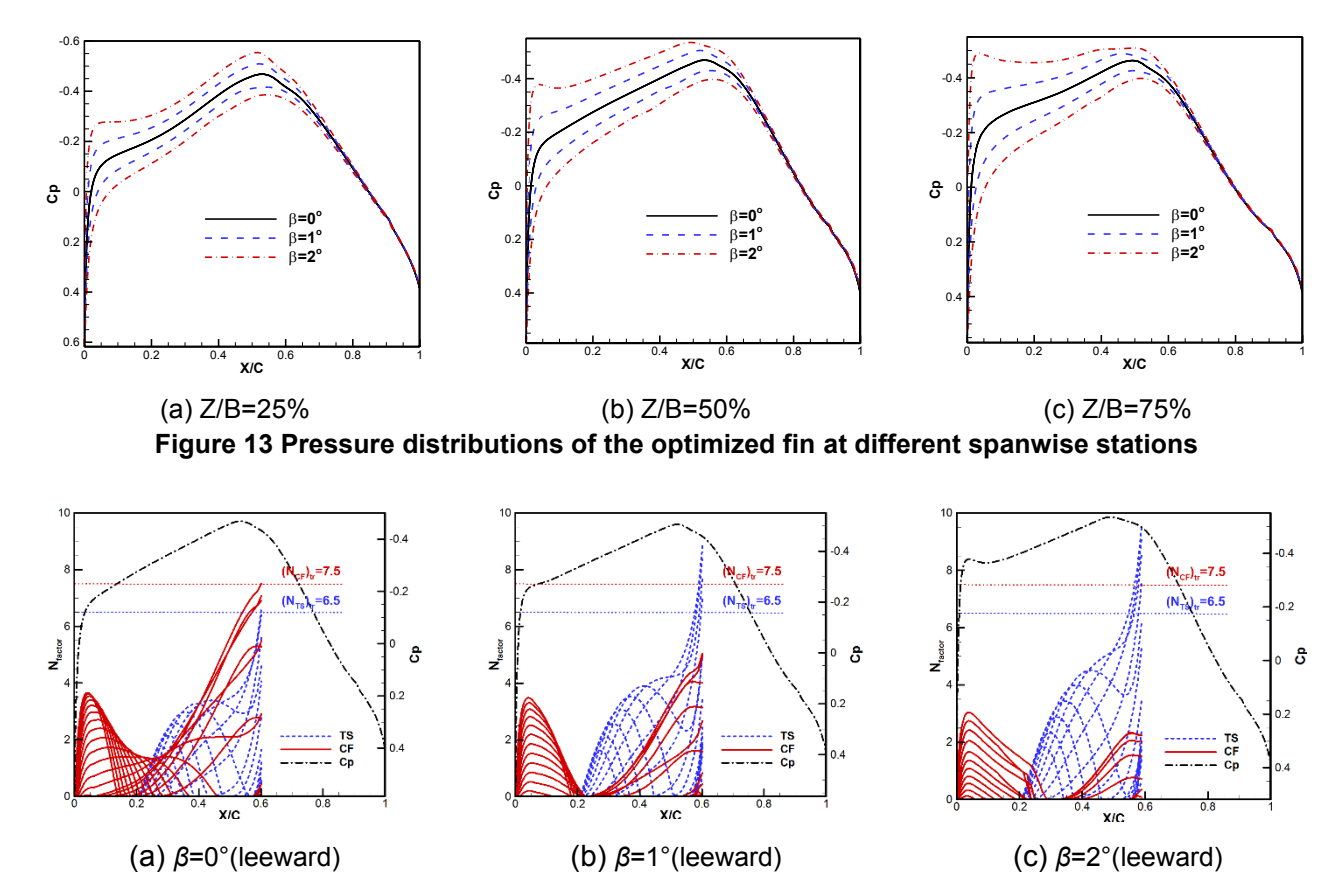


Figure 12 Comparisons of airfoils and suction coefficients for the baseline and the optimized fin

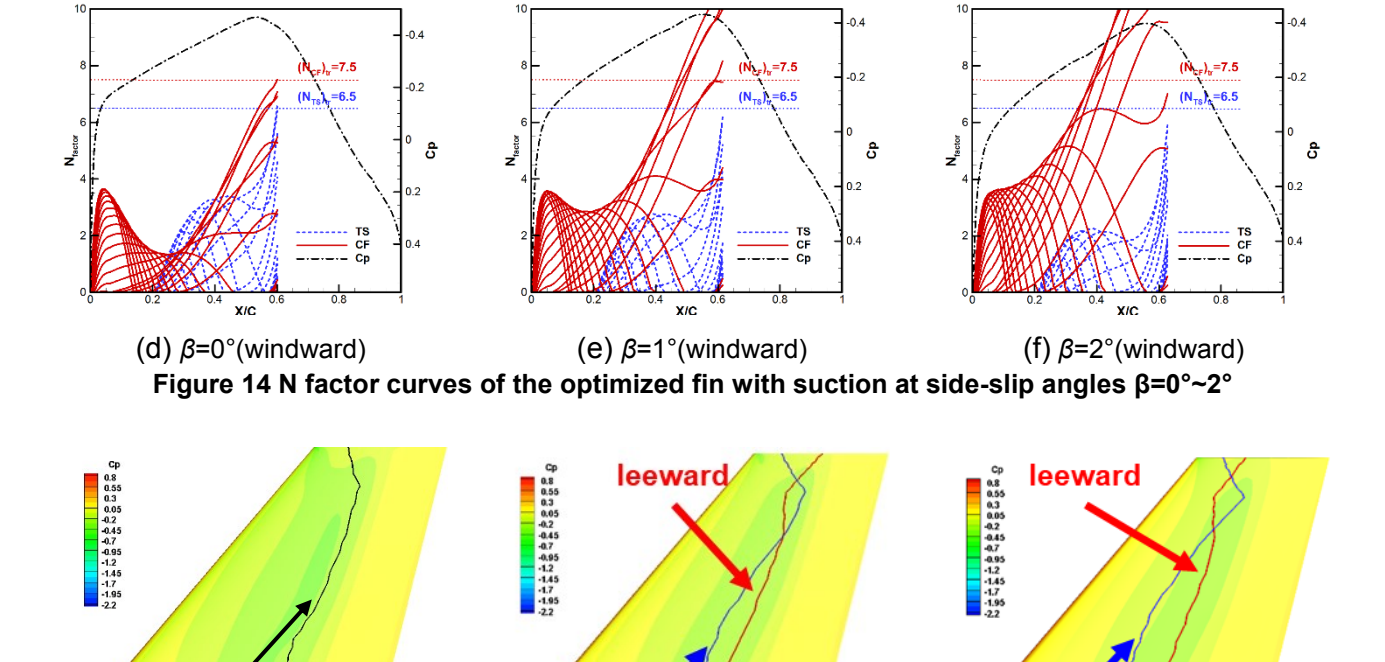
### 3.3 Evaluation of aerodynamic characteristics of the optimized fin configuration

The aerodynamic characteristics of the optimized fin is evaluated at cruise state at different sideslip angles of  $\beta$ =0°~2°. The flow field of the optimized fin is solved and the pressure distributions over the fin surface are presented in **Figure 13**. As can be seen, the favorable pressure gradients are stronger and the ranges of favorable pressure gradient are larger, which can better attenuate the TS instabilities. Stability analysis is conducted on the optimized fin and **Figure 14** demonstrates the *N* factors of TS and CF instabilities over the fin surface. Due to stronger suction near the leading edge, the CF instabilities are well-suppressed near the leading edge even at  $\beta$ =2°. In the downstream region, the amplification of TS instabilities become weaker due to the strong favorable pressure gradient. The predicted transition lines in **Figure 15** show that the laminar region on the optimized fin surface become larger than that on the baseline fin at the sideslip angles of  $\beta$ =0°~2°. The aerodynamic characteristics of the optimized fin are summarized in Table 2. It can be seen that the laminar flow area at the cruise states is enlarged from 41.3% on the baseline fin to 57.7% on the optimized fin, with total drag reduced from 35.46 counts to 31.74 counts. At the sideslip states, due to the stronger favorable pressure gradients and stronger suction, the TS and CF instabilities at the windward and leeward sections are both well-suppressed and a laminar flow area over 47% is kept.



Windward

(c)  $\beta$ =2°



(b)  $\beta=1^{\circ}$ Figure 15 Transition lines of the optimized fin with suction at side-slip angles β=0°~2°

Windward

Table 2 Comparison of aerodynamic characteristics of the baseline and optimized fin with suction

| Configuration         | β (°) | Laminar area<br>(Upper Surface) | Laminar area (Lower Surface) | Drag coefficient (cts) |
|-----------------------|-------|---------------------------------|------------------------------|------------------------|
| Baseline with suction | 0     | 41.25%                          | 41.25%                       | 35.46                  |
|                       | 1     | 40.26%                          | 31.15%                       | 45.86                  |
|                       | 2     | 36.39%                          | 20.32%                       | 66.25                  |
| Opt with suction      | 0     | 57.70%                          | 57.70%                       | 31.74                  |
|                       | 1     | 56.61%                          | 52.82%                       | 39.83                  |
|                       | 2     | 53.48%                          | 47.47%                       | 60.48                  |

#### 4. Conclusions

**Transition line** 

(a)  $\beta$ =0°

This paper mainly studied the design optimization of a HLFC fin with complex geometric constraints. Some conclusions can be drawn as follows.

- (1) A surrogate-based design optimization method is developed for the design of suction and aerodynamic shape parameters of an HLFC fin. The developed method can well deal with the geometric constraints and weighted multi-objective optimization problem. Combining adjustment of suction coefficients and aerodynamic shapes, the TS and CF instabilities inside the fin boundary layer can be well suppressed and thus the transition onset is delayed hence lower friction drag is obtained. Besides, the developed method can consider robustness of aerodynamic performance of certain sideslip angles.
- (2) The developed method is validated on a  $40^{\circ}$ -swept fin at Ma=0.785 and  $Re=2.6\times10^{7}$ . Evaluations of the aerodynamic characteristics and boundary-layer stability characteristics of the optimized fin configuration show that the optimized fin moves the maximum thickness location towards the trailing edge to increase the strength and range of favorable pressure gradient, leading to weaker TS instabilities over the fin surface. The suction coefficients are also increased to better attenuate the crossflows at sideslip states. The laminar flow region at the cruise states is enlarged from 41.3% on the baseline fin to 57.7% on the optimized fin, with total drag reduced from 35.46 counts to 31.74 counts. At sideslip angle  $\beta$ =1° and  $\beta$ =2°, a laminar flow region over 47% is also kept. The above results suggest the effectiveness of our method for HLFC fin design.

Further research of our work is about to increase the number of boundary-layer suction sections, so that the suction distribution could become more reasonable and the required suction coefficient could be reduced. In addition, the energy consumption caused by suction will also be equivalently converted into drag and taken into account in HLFC fin design.

### 5. Acknowledgement

This work was supported by the National Key Research and Development Program of China under Grant No. 2023YFB3002800 and the Youth Innovation Team of Shaanxi Universities. The work was carried out at National Supercomputer Center in Xi'an, and the calculations were performed on Sugon.

#### 6. Contact Author Email Address

Wen-Ping Song\*, Professor, wpsong@nwpu.edu.cn, corresponding author

# 7. Copyright Statement

The authors confirm that they, and/or their company or organization, hold copyright on all of the original material included in this paper. The authors also confirm that they have obtained permission, from the copyright holder of any third party material included in this paper, to publish it as part of their paper. The authors confirm that they give permission, or have obtained permission from the copyright holder of this paper, for the publication and distribution of this paper as part of the ICAS proceedings or as individual off-prints from the proceedings.

#### References

- [1] Zhu Z Q, Ju S J, Wu Z C. Laminar flow active/passive control technology. *Acta Aeronautica et Astronautica Sinica*, vol. 37, No. 7, pp. 2065-2090, 2016. (in Chinese)
- [2] Henke R. A320 HLFC fin flight tests completed. Air & Space Europe, Vol. 1, No. 2, pp. 76-79, 1999.
- [3] Schrauf G H. Evaluation of the A320 hybrid laminar fin experiment. *European Congress on Computational Methods in Applied Sciences and Engineering*, ECCOMAS, 2000.
- [4] Dziomba B. European Laminar Flow Projects. *2nd Community Aeronautics RTD Conference*: Aerodays, Naples, 1993.
- [5] Jabbal M, Everett S, Krishnan K S G, Raghu S. A comparative study of hybrid flow control system architectures for an A320 aircraft. 8th AIAA Flow Control Conference, 2016.
- [6] Andrea C, Simon L, Peter W, Mohammed S M. Aerodynamic and transition analysis of the hybrid laminar flow controlwing at ARA wind tunnel. *AIAA Aviation 2019 Forum*, 2019.
- [7] Schrauf G, Geyr, H V. Simplified Hybrid Laminar Flow Control for the A320 Fin Aerodynamic and System Design, First Results. *AIAA SciTech Forum and Exposition*, 2020.
- [8] Schrauf G, Geyr, H V. Simplified Hybrid Laminar Flow Control for the A320 Fin. Part 2: Evaluation with the eN-method. *AIAA Science and Technology Forum and Exposition*, pp 1-21, 2021.
- [9] Schrauf G, Geyr, H V. Hybrid laminar flow control on a320 fin: Retrofit design and sample results. *Journal of Aircraft*, Vol. 58, No. 6, pp 1272-1280, 2021.
- [10]Yang T H, Bai J Q, Shi Y Y, Yang Y X, Lu L. Optimization design for HLFC wings considering influence of suction distribution. *Acta Aeronautica et Astronautica Sinica*, Vol. 38, No. 12, 2017. (in Chinese)
- [11]Xie F T, Song W P, Han Z H. Numerical study of high-resolution scheme based on preconditioning method. *Journal of Aircraft*, Vol. 46, No. 2, pp 520-525, 2009.
- [12]Zhang K, Song W P. Infinite Swept-wing Reynolds-averaged Navier-stokes Computations with Full e<sup>N</sup> transition criterion. *27th Congress of the International Council of the Aeronautical Sciences*, Nice, France, 2010.
- [13]Zhu Z, Song W P, Han Z H. Automatic transition prediction for wing-body configurations using dual e<sup>N</sup> method. *Acta Aeronautica et Astronautica Sinica*, Vol. 39, No. 2, 2018. (in Chinese)
- [14]Mack L M. Stability of three-dimensional boundary layers on swept wings at transonic speeds. Symposium Transsonicum, pp 209-225, 1988.
- [15]Arnal D. Boundary layer transition: Predictions based on linear theory. AGARD, 1994.
- [16]Han Z H. SurroOpt: A Generic Surrogate-based Optimization Code for Aerodynamic and Multidisciplinary Design, 30th Congress of the International Council of the Aeronautical Sciences, Daejeon, Korea, 2016.
- [17]Kulfan B M. Universal parametric geometry representation method. *Journal of Aircraft*, vol. 45, No.1, pp. 142-158, 2008.
- [18] Giunta, Anthony A, Wojtkiewicz Jr, Steven F, Eldred, Michael S. Overview of modern design of experiments methods for computational simulations. *41st Aerospace Sciences Meeting and Exhibit.* 2003.

## Boundary-layer Suction and Aerodynamic Shape Optimization for HLFC on a Fin

[19]McKay M D, Beckman R J, Conover W J. A comparison of three methods for selecting values of input variables in the analysis of output from a computer code, *Technometrics*, Vol. 21, No. 2, pp. 239-245, 1979.

[20]Liu J, Song W P, Han Z H, Zhang Y. Efficient aerodynamic shape optimization of transonic wings using a parallel infilling strategy and surrogate models, *Structural and Multidisciplinary Optimization*, Vol. 55, No. 3, pp 925-943, 2017.